12th International Conference on Fracture Mechanics of Concrete and Concrete Structures
FraMCoS-12
B.L.A. Pichler, Ch. Hellmich, P. Preinstorfer (Eds)
https://doi.org/10.21012/FC12.1233
TT-C2:5

BLAST LOADING EFFECT OF EXPLOSIVE WEIGHT DISTRIBUTION ON RC COLUMNS

Md Imran Mohnavi[1#], G Appa Rao[2]

[1] PhD Student, Department of Civil Engineering, Indian Institute of Technology, Madras, email:imranmohnavi@gmail.com

[2]Professor, Department of Civil Engineering, Indian Institute of Technology, Madras, email:garao@zmail.iitm.ac.in

Chennai 600036, India

Keywords: Blast, Explosion, Concrete Column, Damage Propagation, Explosive Weight Distribution.

Abstract: Explosive effects are commonly encountered on structures. The 2020 Beirut explosion, 9/11 attack in USA, or current Russia-Ukraine war cause significant structural destruction. Reinforced concrete (RC) members in compression are most vulnerable to blast loads. This paper deals with a numerical investigation on the propagation of damage and its effects due to distribution of explosives at different positions around a compression member for close range explosion. In this analysis, explosive weight and scaled distance are maintained constant throughout. The Arbitrary Lagrange Euler (ALE) algorithm along with Fluid-Structure Interaction (FSI) and Erosion algorithms, to accurately capture the blast effects have been employed. Models have been validated by assessing the damage profile and blast over-pressure. The concrete and reinforcement have been modeled using the Lagrange approach, while Eulerian method is adopted to model air and explosives. Coupling between the Lagrange and Eulerian part have been considered along with the contact between concrete and reinforcement. The strain contour reveals that damage propagation in a compression member varies with its cross-sectional size and the placement of explosives. Compression members with larger cross-sections exhibit a pronounced effect of explosive distribution, with damage penetrating to the core from the explosion side. In contrast, compression members with small cross-sections show reduced effectiveness of explosive distribution due to the small cross section size. In C900, plastic strain extends toward the core from the side of the explosion, whereas in C450, damage reaches the core from the opposite side of the explosion, leading to complete failure of compression member.

1. INTRODUCTION

In recent years, significant progress has been made in many underdeveloped countries, with infrastructure growth often serving as a key indicator of a nation's advancement. Infrastructure encompasses elements such as flyovers, bridges, nuclear plants, thermal power stations, and buildings of national significance. Among the infrastructure parts, columns play vital role in the structural integrity of both bridges and buildings. The failure of a column can trigger a chain reaction of progressive collapse, potentially leading to the complete destruction of the structure. This critical role has made columns a focal point for extensive research. In addition to bearing static loads, columns are also exposed to dynamic impact loads, such as those resulting from vehicle collisions or explosions, throughout their lifespan. In recent years, numerous countries have been engaged in conflicts, leading to a surge in the use of ammunition and explosives. This escalation leads to increase in the production and consumption of arms, significantly impacting national economies.

To sustain prolonged engagements and minimize economic strain, the strategic utilization of explosives becomes essential. Previous studies have predominantly examined scenarios involving a single blast source, with all explosives concentrated at one point, aiming at analysing the column behaviour and proposing mitigation strategies along with design enhancements. In contrast, this study focuses on the behaviour of reinforced concrete columns subjected to explosions, emphasising on a fixed quantity of explosives distributed and positioned around the column.

2. LITERATURE REVIEW

Square-shaped columns have been found to be more susceptible to non-contact blasts compared to circular columns, exhibiting damage characteristics such as core concrete loss, stirrup failure, and spalling of cover concrete [1]. Increase in longitudinal and transverse reinforcement has been found to enhance the column residual axial capacity [2]. Piers designed for seismic loads demonstrate superior performance compared to conventionally designed piers. Additionally, surface explosions are observed to cause greater damage than free-air bursts [3]. The failure mode transitions from local to global with the standoff distance increment for the same explosive weight. Local shear damage is observed at the base, while global flexural damage occurs in the middle of the pier for small and large scaled distance explosions, respectively [4]. For low explosive weights and the same scaled distance, the column response is unaffected by the transverse reinforcement detailing. Additionally, the scaled distance has a greater influence on the column's damage profile than the explosive weight [5]. Equations have been suggested to estimate the residual axial capacity of a column for any given explosive weight [6]. Increasing the concrete grade enhances the pier's resistance, while increasing the pier diameter does not contribute to improving its resistance [7]. Vehicle collision followed by an explosion was studied and found the sequence represents the most critical loading condition, leading to direct shear failure. The impact of the collision depends on the vehicle's velocity, while the blast's effect is influenced by the scaled distance [8]. A critical combination of scaled distance and axial load has been identified that maximizes the column's vulnerability [9]. Sequential blast and impact loading were conducted for various loading locations, revealing that the Impact-Blast and Blast-Impact sequences are the most destructive for both close and distant explosions at the same height. However, for different heights in a close field, the Impact-Blast sequence is more devastating, while in the far field, both sequences have the same effect [10]. Precast concrete members with steel tubes perform better than those without steel tubes, and the explosive location influences the resistance capacity of the member [11]. Rectangular columns perform better than square columns, and increasing the width helps in enhancing the resistance to blast loading by reducing the extent of the damage [12]. Spall damage was classified into threshold, medium, and severe levels, with the finding that the extent of spall damage is independent of the column height and boundary conditions [13]. Reinforcement aids in resisting blast loading [2-13]. At same scaled distance, the deflection and extent of damage are significantly greater for double-end initiation compared to single-point initiation of an explosive [14]. The explosive shape and the detonation method influences the failure characteristics of columns [14]. Under blast loading, variable axial load causes larger displacements along the column height compared to constant axial loads. Columns subjected to variable axial loads experience gradual and progressive damage, while those under constant axial loads undergo concrete crushing, leading to failure [15]. Close-in blast to column causes local damage like spallation and crushing of concrete [16].

Increase in axial load enhances the pier's resistance in its design [3-14]. Lower stirrup spacing improves column response to blast load [7-16]. Depth increment safeguards column against blast [13-16].

3. MODELLING DETAILS

3.1. Numerical Model Validation

Numerical models were validated against the experimental findings from the thesis entitled "Near-Field Explosion Effects on Reinforced Concrete Columns: An Experimental Investigation" [19]. A mesh sensitivity analysis was conducted using air domain mesh sizes of 30, 35, 40, and 45mm, with the 40mm mesh size providing the closest results of 38,200 kPa and 1,540 kPa at the place of bottom and top pressure gauges, as shown in Figure 1. During this process, the blast overpressure parameters were validated to ensure the accuracy of the Eulerian component of the model, while the Lagrangian component was validated by comparing the column's damage profile of different sides i.e. (a & b) front and right-side face, (c) back and left side face as depicted in Figures 2. and 3.

3.2.Material Model

Concrete: The concrete material adopted is Karagozian & Case (K&C) model using Keyword MAT_CONCRETE_DAMAGE_REL3

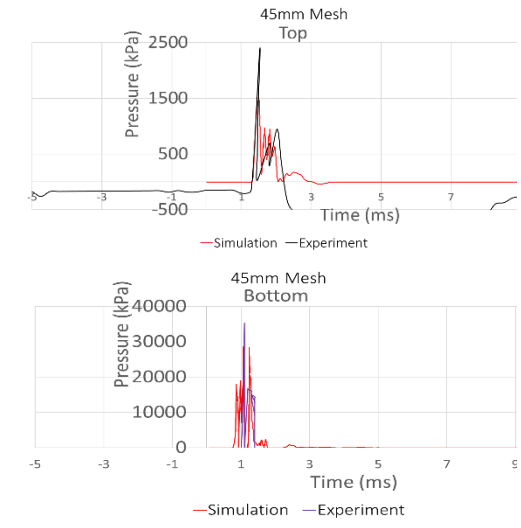

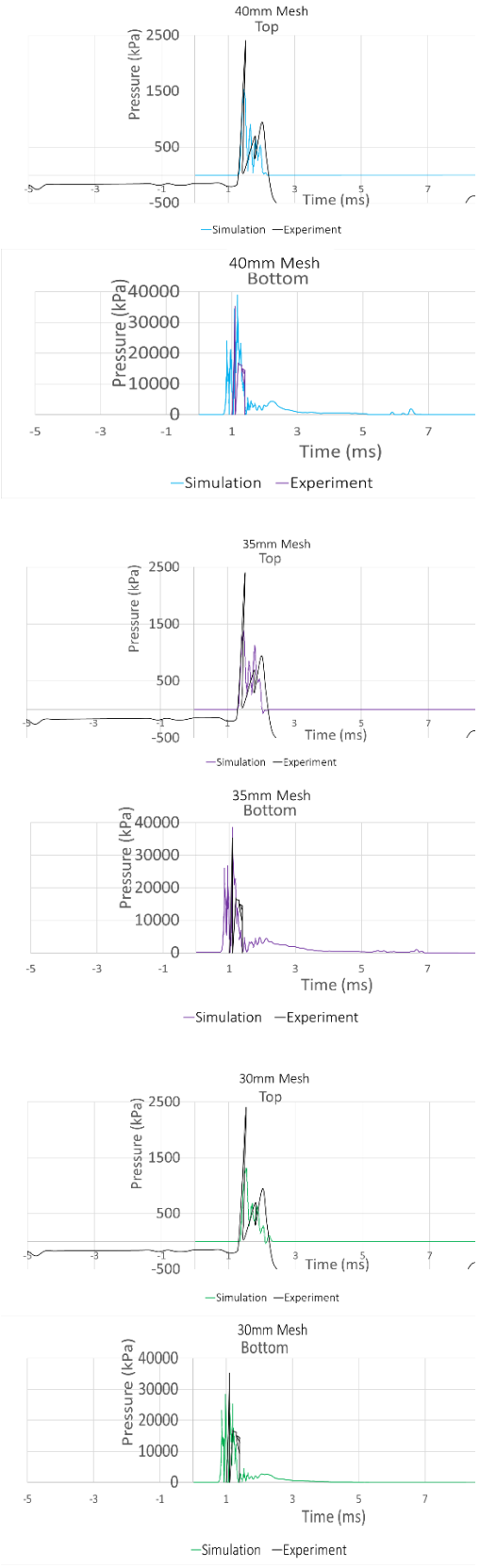

Figure 1: Mesh Sensitivity Analysis

Figure 2: Experimental Post-Blast Damage [19]

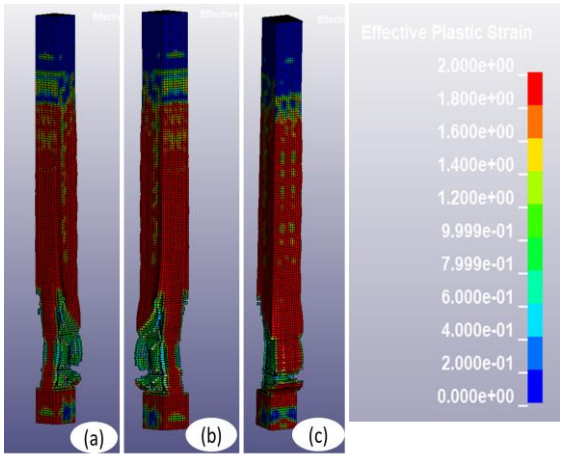

Figure 3: Numerical Post-Blast Damage

(Mat_72R3) in LSDYNA with parameters listed in Table 1. It incorporates three failure surfaces i.e. yield, ultimate and residual with consideration of strain rate effect and stiffness degradation. The advantage of this model is the automatic generation of its parameters with single user input i.e. unconfined compressive strength of concrete. High loading rate causes increase in the material strength which were incorporated in the model using Dynamic Increase Factor (DIF) defined as the ratio of dynamic and static compressive strength of concrete at high and quasi-static strain rate. The DIF equations for compressive and tensile strength are adopted from CIB-FIP Model Code 1990 [17] as shown below:

For Tension,

$$DIF_T = \left(\frac{\dot{\varepsilon}}{\dot{\varepsilon}_s}\right)^{1.016\delta} \quad \dot{\varepsilon} \le 30/sec$$
$$= \beta\left(\frac{\dot{\varepsilon}}{\dot{\varepsilon}_s}\right)^{\frac{1}{3}} \quad \dot{\varepsilon} > 30/sec \quad \ldots\ldots(1)$$

With $\beta = 10^{7.112\delta - 2.33}$ and $\delta = \frac{1}{10+6\frac{f_c}{f_{co}}}$

Where $\dot{\varepsilon}$ is the current strain rate, $\dot{\varepsilon}_s = 3 \times 10^{-6}/\text{sec}$ is the reference strain rate.

For Compression,

$$DIF_C = \left(\frac{\dot{\varepsilon}}{\dot{\varepsilon}_s}\right)^{1.026\alpha} \quad \dot{\varepsilon} \le 30/sec$$
$$= \gamma\left(\frac{\dot{\varepsilon}}{\dot{\varepsilon}_s}\right)^{\frac{1}{3}} \quad \dot{\varepsilon} > 30/sec \quad \ldots\ldots(2)$$

With $\gamma = 10^{6.15\alpha - 2}$ and $\alpha = \frac{1}{5+9\frac{f_c}{f_{co}}}$

Where $\dot{\varepsilon}$ = current strain rate, $\dot{\varepsilon}_s = 3 \times 10^{-5}/\text{sec}$ is the reference strain rate.

Where f_c = unconfined compressive/tensile strength of concrete to be determined (MPa), f_{co} = 10 MPa

The change in concrete volume due to pressure is described using the Equation of State with the keyword EOS_TABULATED_COMPACTION, which establishes the relationship between pressure and volumetric strain.

Steel: The steel material as reinforcement is defined using the keyword MAT_PLASTIC_KINEMATIC, which accounts for both isotropic and kinematic hardening effects with parameters listed in Table 1. The strain rate effect is considered using the Cowper-Symonds (CS) model [18], with the Dynamic Increase Factor (DIF) equation as $DIF = 1 + \left(\frac{\dot{\varepsilon}}{C}\right)^{\frac{1}{P}}$ where $\dot{\varepsilon}$ is the strain rate, C and P are the strain rate parameters.

Air: It is modelled using the Multi-Material Arbitrary Lagrangian Eulerian (MMALE) formulation as a non-viscous ideal fluid using the keyword MAT_NULL. The Equation of State is defined with the keyword EOS_LINEAR_POLYNOMIAL, which is expressed as a linear polynomial, allowing the material to behave with zero

shear stiffness and follow the pressure equation given as

$$P = C_0 + C_1\mu + C_2\mu^2 + C_3\mu^3 + (C_4 + C_5\mu + C_6\mu^2)E \quad \ldots\ldots\ldots\ldots(3)$$

Where C_0 to C_6 are polynomial equation coefficients, $\mu = \frac{\rho}{\rho_0} - 1$ denotes the volumetric strain (where ρ and ρ_0 are reference and current density respectively), E is the internal energy and V_0 is the relative volume. The input parameters are listed in Table 1.

TNT: Its domain is modelled by MMALE concept with MAT_HIGH_EXPLOSIVE_BURN keyword, which simulates the rapid detonation process and the high pressures generated by the explosion. This model works in conjunction with Jones-Wilkins-Lee (JWL) Equation of State EOS_JWL, which describes the pressure of the detonation products as a function of their specific volume and internal energy as shown below with the input parameters listed in Table 1.

$$P = A\left(1 - \frac{\omega}{R_1 V}\right)e^{-R_1 V} + B\left(1 - \frac{\omega}{R_2 V}\right)e^{-R_2 V} + \frac{\omega E}{V} \quad \ldots\ldots(4)$$

where A, B are constants with units of pressure, E is the detonation energy per unit volume, V is the initial relative volume and R_1, R_2 & ω are unit-less constants.

3.3. Model Specifications

The models were developed in LS-DYNA software using the Multi-Material Arbitrary Lagrange Eulerian (MMALE) method, consisting of Eulerian and Lagrangian parts. The Lagrangian component represents concrete and steel, while the Eulerian component includes air and explosive materials. To address computational constraints and ensure mesh convergence, a mesh size of 20 mm was used for the column, and 40 mm for the air domain. The study includes two reinforced concrete (RC) columns with circular cross-sections, designated as C900 and C450, constructed using M40 grade concrete and Fe415 steel, as detailing in Figure 4.

Table 1: Material Model Input Parameters

CONCRETE			
Density (ρ)	Compressive Strength	Maximum Failure principal strain	
2400 kg/m^3	40 MPa	0.15	

STEEL				
Density (ρ)	Elastic Modulus (E)	Poisson Ratio (υ)	Strain Rate Parameter	
			C	P
7850 kg/m^3	206 GPa	0.3	40 s^{-1}	5 s^{-1}
Failure Strain				
0.14				

AIR		
Initial Density (ρ)	Initial Energy (E_0)	Pressure Cutoff
1.29 kg/m^3	2.5 x 10^5 J/m^3	0
C_0,C_1,C_2,C_3,C_6	C_4, C_5	
0	0.4	

TNT			
Initial Density (ρ)	Detonation Velocity (V_d)	Burst Pressure (P_{CJ})	A (GPa)
1630 kg/m^3	6930 m/s	21 GPa	373.8
B (GPa)	E_0 (J/m^3)	ω	V
3.747	6 x 10^9	0.35	1
R_1	R_2		
4.15	0.9		

Concrete is modelled using solid elements, while steel is represented using beam elements, both with single-point integration. Air is modelled as a solid element with non-reflecting boundaries to prevent reflections. The finite element model is illustrated in Figure 5.

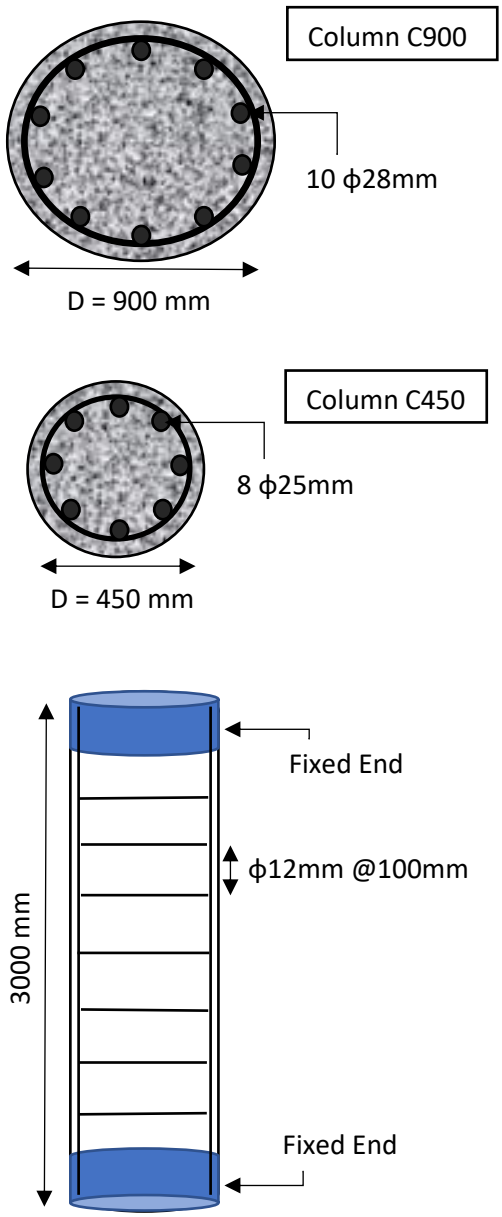

Figure 4: Column Detailed Configuration

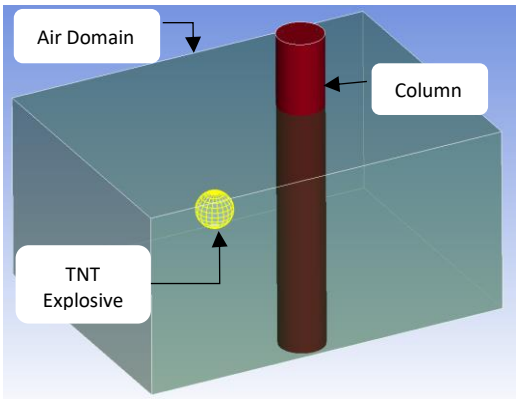

Figure 5: Finite Element Model Depiction

A spherical shape explosive of 100kg Trinitrotoluene (TNT) is modelled to simulate the blast. The size and shape of the explosive were defined using the keyword INITIAL VOLUME FRACTION GEOMETRY. The placement and distribution of the explosive were designed to maintain a constant scaled distance of 0.2 m/kg$^{1/3}$, ensuring a close-field explosion, as illustrated in Figure 6, as mentioned in Table 2.

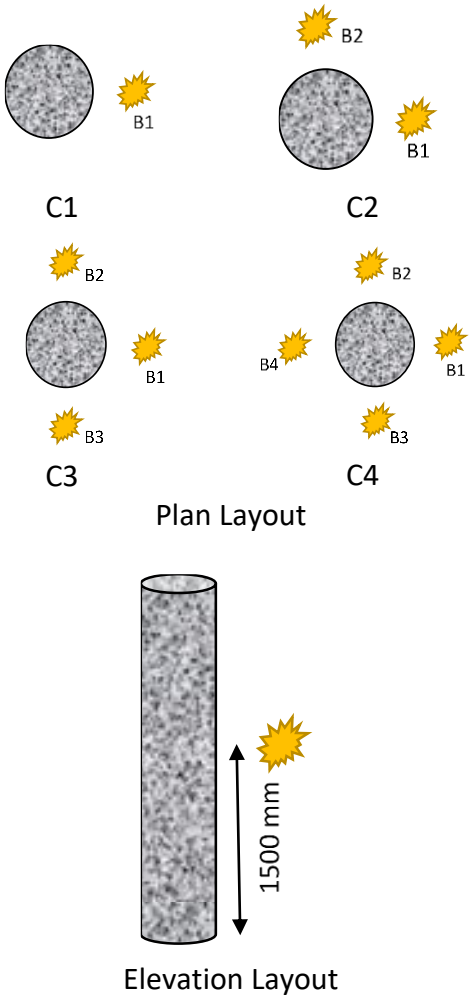

Figure 6: Explosive Distribution Cases

Table 2: Explosive Distribution Details

Explosion Cases	Explosive Weight Distribution (kg)
C1 (B1)	100
C2 (B1, B2)	50
C3 (B1, B2, B3)	33.33
C4 (B1, B2, B3, B4)	25

The interaction between concrete and steel is modelled using the keyword CONTACT AUTOMATIC SURFACE TO SURFACE, with a friction coefficient of 0.4. The coupling of the Lagrangian and Eulerian parts is achieved using the keyword CONSTRAINED BEAM IN SOLID, incorporating fluid-structure interaction within the model. The column self-weight is applied at the ends as a constant axial load using the keyword LOAD BODY.

4. RESULTS AND DISCUSSION

4.1. Damage Propagation

The damage progression of column cross-section is monitored at the column's mid-height over five times intervals of 0.25 ms beginning at 0.5 ms when the blast wave first strikes the column and continuing up to 1.5 ms covering the blast's positive phase. For C450 column, damage initially originates on the explosion-facing side and propagates around the column's periphery, eventually causing deeper damage from the side opposite to the blast as shown in Figures 7-10.

- C450C1: Begins damage with partial cover loss on the explosion-facing side, accompanied by minor in-depth damage. Major damage occurs on the rear side of the column because of being tension side, affecting approximately 50% of the cross-section as shown in Figure 7.
- C450C2: Sustains minor peripheral damage, with major damage initiating on the side opposite to the blast wave overlap. This occurs due to tension generated by a larger resultant overlapped force in that direction ultimately affecting approximately 70% of the cross-section as shown in Figure 8.
- C450C3: Sustains minor peripheral damage initially, with major damage starting on the non-explosive side, similar to C500C1. However, the effects of overlapping blasts cause a slight shift in the damage initiation point, resulting in extensive damage that affects approximately 80% of the cross-section as shown in Figure 9.

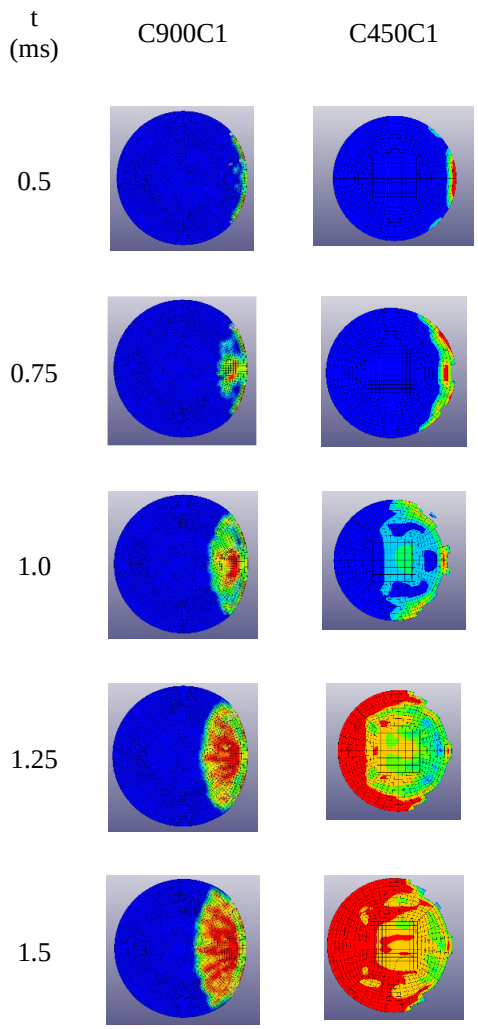

Figure 7: Damage Propagation for C1 Case

- C450C4: Clearly demonstrates the effect of blast wave overlap, resulting in the formation of a concentric circular damage pattern at 1.25 ms, ultimately leading to complete failure of column's cross-section as shown in Figure 10.

In column C900, the blast wave overlap effect is not observed in any of the cases. Damage initiation and propagation occur solely from the explosion-facing side.

- C900C1: Damage begins on the explosion-facing side, without damaging the column core as shown in Figure 7.

- C900C2: Damages approximately 50% of the cross-section, including half of the column core as shown in Figure 8.

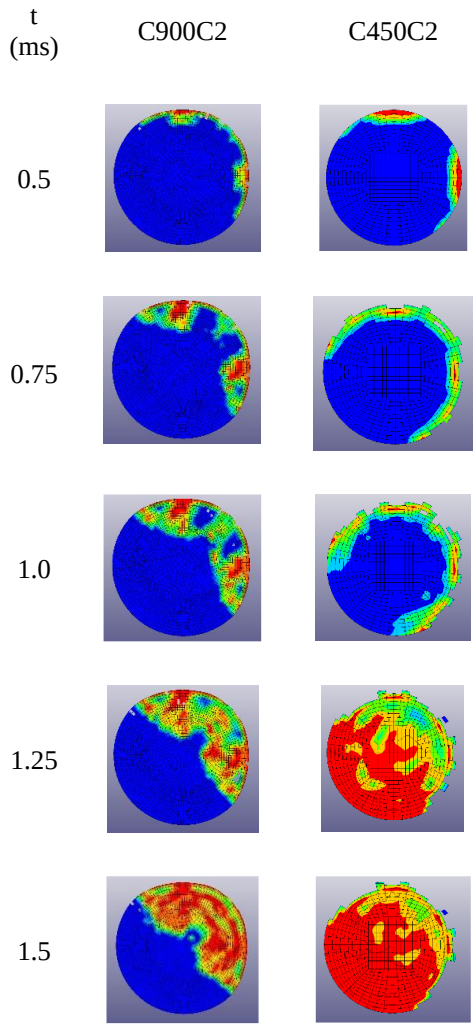

Figure 8: Damage Propagation for C2 Case

- C900C3: Significant in-depth damage, affecting nearly 75% of the cross-section, with major damage to the core as shown in Figure 9.
- C900C4: Peripheral damage propagation, leading to maximum in-depth minor damage as shown in Figure 10.

4.2.Pressure Wave Propagation

From the initiation of the explosion to the wave striking the column, the pressure wave propagation is similar across all cases of C900 and C450, with the C4 case shown in Figure 11.

After the column-wave interaction, the behaviour diverges. In C450, the wave fully engulfs the column from all sides, due to the relatively small size of the column compared to the blast wave. The overlapping of the blast wave significantly contributes to the damage, as seen in C450C2. In contrast, in C900, the larger cross-sectional area of the column limits the wave's ability to damage only those regions it directly contacts.

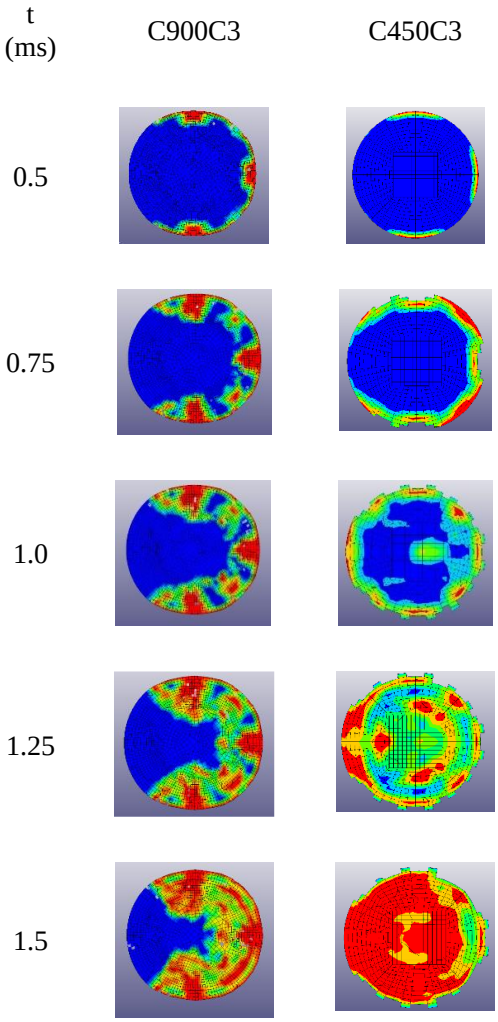

Figure 9: Damage Propagation for C3 Case

5. CONCLUSION

- Among the blast cases analysed for C900, C4, C3, and C2 exhibit greater damage compared to C1, with varying depths of damage across these cases. However, the total deformation contour is the highest in the C4 case, indicating that the explosive distribution method is

effective in large cross-section columns.

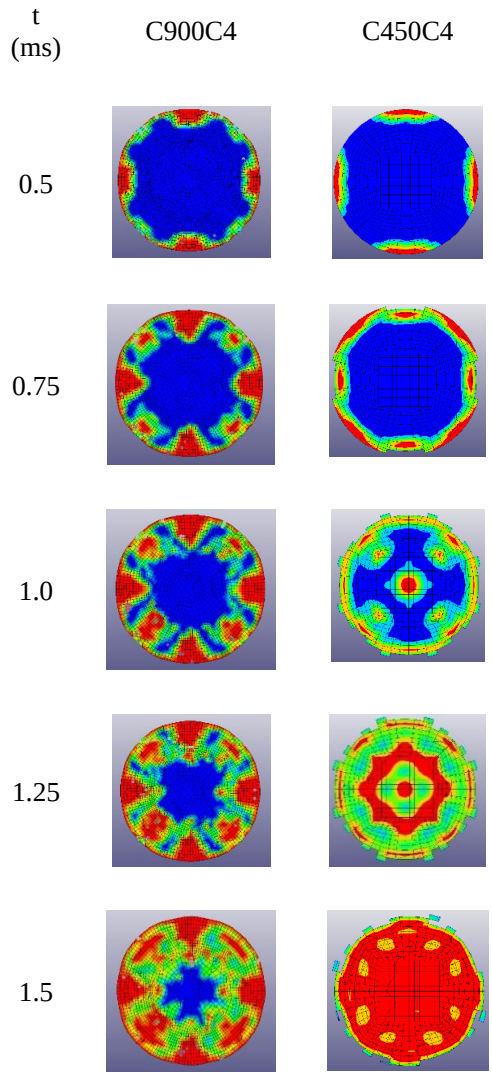

Figure 10: Damage Propagation for C4 Case

- For the cases of C450, the explosive distribution method is not highly effective, as more than 50% of the cross-section is damaged in all cases, rendering the column incapable of carrying further loads.
- The propagation of blast pressure waves indicates that the column size and the blast wave size must be comparable for the explosive distribution method to be effective. This can be achieved by limiting the explosive amount, taking the column size into consideration. Excess amount of explosive for distribution for small cross-section columns essentially results in a high-magnitude single-source blast, which is more intense than the intended effect of distributed explosives. The explosive distribution technique is not always effective; its success depends on factors such as the explosive weight, positioning, and the size of the column.

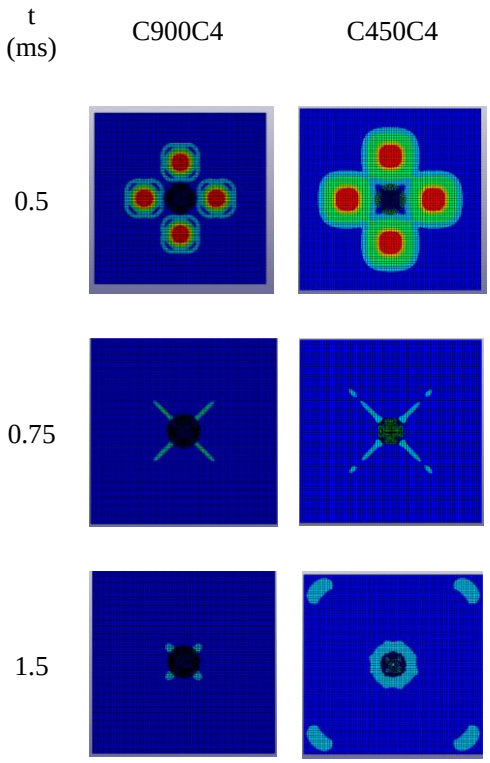

Figure 11: Wave Propagation in Air Domain

6. REFERENCES

[1] Yuan, S., Hao, H., Zong, Z. and Li, Jun, 2017. A Study of RC Bridge Columns under Contact Explosion. International Journal of Impact Engineering, vol. 109, Elsevier BV, Nov. 2017, pp. 378–90.

[2] Xu, J.P., Wu, H., Ma, L.L. and Fang, Q. 2022. Residual Axial Capacity of Seismically Designed RC Bridge Pier after Near-range Explosion of Vehicle Bombs. Engineering Structures, vol. 265, Elsevier BV, Aug. 2022, p. 114487.

[3] Patel, K., Goswami, A. and Adhikary, S.D., 2020. Response Characterization of Highway Bridge Piers Subjected to Blast Loading. Structural Concrete, vol. 21, no. 6, Wiley, May 2020, pp.

2377–95.

[4] Chenxu, Lv, Yan, Q., Li, Liang and Li, Shutao, 2023. Field Test and Probabilistic Vulnerability Assessment of a Reinforced Concrete Bridge Pier Subjected to Blast Loads. Engineering Failure Analysis, vol. 143, Elsevier BV, Jan. 2023, p. 106802.

[5] Kyei, Conrad and Braimah, Abass. 2017. Effects of Transverse Reinforcement Spacing on the Response of Reinforced Concrete Columns Subjected to Blast Loading. Engineering Structures, vol. 142, Elsevier BV, July 2017, pp. 148–64.

[6] Liu, L., Zong, Z.H. and Li, M.H., 2018. Numerical Study of Damage Modes and Assessment of Circular RC Pier under Noncontact Explosions. Journal of Bridge Engineering, vol. 23, no. 9, American Society of Civil Engineers (ASCE), Sept. 2018.

[7] Ma, L.L., Wu, H., Fang, Q. and Xu, J.P. 2022. Displacement-based Blast-resistant Evaluation for Simply-supported RC Girder Bridge under Below-deck Explosions. Engineering Structures, vol. 266, Elsevier BV, Sept. 2022, p. 114637.

[8] Fang, Chen, Yosef, T.Y., Linzell, D.G. and Rasmussen, J.D. 2021. Computational Modeling and Dynamic Response of Highway Bridge Columns Subjected to Combined Vehicle Collision and Air Blast. Engineering Failure Analysis, vol. 125, Elsevier BV, July 2021, p. 105389.

[9] Shi, Y., Hu, Ye, Chen, Li, Li, Z.X. and Xiang, Hengbo, 2022. Experimental Investigation into the Close-in Blast Performance of RC Columns with Axial Loading. Engineering Structures, vol. 268, Elsevier BV, Oct. 2022, p. 114688.

[10] Gholipour, G., Zhang, C. and Mousavi, A.A., 2020. Numerical Analysis of Axially Loaded RC Columns Subjected to the Combination of Impact and Blast Loads. Engineering Structures, vol. 219, Elsevier BV, Sept. 2020, p. 110924.

[11] Do, Tin V, Pham, T.M. and Hao, Hang, 2020. Stress Wave Propagation and Structural Response of Precast Concrete Segmental Columns under Simulated Blast Loads. International Journal of Impact Engineering, vol. 143, Elsevier BV, Sept. 2020, p. 103595.

[12] Dua, A., Braimah, A. and Kumar, M., 2020. Experimental and Numerical Investigation of Rectangular Reinforced Concrete Columns under Contact Explosion Effects. Engineering Structures, vol. 205, Elsevier BV, Feb. 2020, p. 109891.

[13] Li, Jun and Hao, Hong, 2014. Numerical Study of Concrete Spall Damage to Blast Loads. International Journal of Impact Engineering, vol. 68, Elsevier BV, June 2014, pp. 41–55.

[14] Chen, Li, Hu, Ye, Ren, Huiqi, Xiang, Hengbo, Zhai, Chaochen, and Fang, Qin, 2019. Performances of the RC Column Under Close-in Explosion Induced by the Double-end-initiation Explosive Cylinder. International Journal of Impact Engineering, vol. 132, Elsevier BV, Oct. 2019, p. 103326.

[15] Abebe, Solomon and Getachew, Solomon, 2022. Numerical Study on Effect of Constant and Variable Axial Loads on RC Column Subjected to Blast Load. Heliyon, vol. 8, no. 11, Elsevier BV, Nov. 2022, p. e11681.

[16] Cui, J., Shi, Y., Li, Z. X., and Chen, L. 2015. Failure analysis and damage assessment of RC columns under close-in explosions. Journal of Performance of Constructed Facilities, 29(5), B4015003.

[17] Comité Euro-International du Béton (CEB). CEB-FIP Model Code 1990: Design Code. Thomas Telford Publishing.

[18] Cowper, G., and Symonds, P., 1957. Strain Hardening and Strain-Rate Effects in the Impact Loading of Cantilever Beams. Brown University,

Division of Applied Mathematics.
[19] Siba, F., 2014. Near-field explosion effects on reinforced concrete columns: An experimental investigation, Master's thesis, Carleton University, Ottawa, Ontario.